Journal of Nuclear Materials 384 (2009) 292–302

Contents lists available at ScienceDirect

Journal of Nuclear Materials

journal homepage: www.elsevier.com/locate/jnucmat

Protection of nuclear graphite toward fluoride molten salt by glassy carbon deposit

V. Bernardet [a], S. Gomes [b], S. Delpeux [c], M. Dubois [b], K. Guérin [b], D. Avignant [b], G. Renaudin [b], L. Duclaux [a,*]

[a] LCME, Polytech'Savoie, Université de Savoie, Campus de Savoie Technolac, 73376 Le Bourget du Lac cedex, France
[b] LMI, UMR CNRS 6002, Université Blaise Pascal and Ecole Nationale Supérieure de Chimie de Clermont-Ferrand, 24 Avenue des Landais, 63177 Aubière cedex, France
[c] CRMD, CNRS, 1B Rue de la Férollerie 45071 Orléans cedex 2, France

ARTICLE INFO

Article history:
Received 2 June 2008
Accepted 28 November 2008

ABSTRACT

Molten salt reactor represents one of the promising future Generation IV nuclear reactors families where the fuel, a liquid molten fluoride salt, is circulating through the graphite reactor core. The interactions between nuclear graphite and fluoride molten salt and also the graphite surface protection were investigated in this paper by powder X-ray diffraction, micro-Raman spectroscopy and scanning electron microscopy coupled with X-ray microanalysis. Nuclear graphite discs were covered by two kinds of protection deposit: a glassy carbon coating and a double coating of pyrolitic carbon/glassy carbon. Different behaviours have been highlighted according to the presence and the nature of the coated protection film. Intercalation of molten salt between the graphite layers did not occur. Nevertheless the molten salt adhered more or less to the surface of the graphite disc, filled more or less the graphite surface porosity and perturbed more or less the graphite stacking order at the disc surface. The behaviour of unprotected graphite was far to be satisfactory after two days of immersion of graphite in molten salt at 500 °C. The best protection of the graphite disc surface, with the maximum of inertness towards molten salt, has been obtained with the double coating of pyrolitic carbon/glassy carbon.

1. Introduction

The development of the fourth generation molten salt breeder reactors might enable to reduce the nuclear waste treatment [1–3]. In these reactors, the molten salt (mixture of fluorides composed mainly of NaF, LiF, ZrF_4, ThF_4 and UF_4) used both as fuel and coolant, flows between the reactor core made of graphite and the heat exchanger. The development of molten salt breeder reactor requires studies of the compatibility at high temperature of the graphite core with the molten salt environment. The viability of the molten salt reactor supposes inertness behaviour of graphite toward the liquid fluoride fuel, no corrosion phenomena of the graphite and no interaction with the fluoride molten salt in the operating conditions.

We have studied the reactivity of nuclear graphite toward the ternary fluoride molten salt of eutectic composition: 27 mol.% (molar %) LiF, 36.5 mol.% NaF and 36.5 mol.% ZrF_4. Introduction of fissile UF_4 and ThF_4 in the molten salt in the operating conditions will not modify fluoride salt behaviour due to their crystallochemical properties analogous to ZrF_4. The reactivity of graphite was studied in term of possible formation of graphite intercalation compounds, adherence phenomena, graphite surface porosity filling by fluoride salts, and diffusion of fluoride into the graphite. The contact of graphite samples with the molten salt was achieved by immersion of the graphite discs in the molten salt at 500 °C for 2 days in an inert nitrogen atmosphere. Two kinds of graphite coating have been envisaged in order to improve its inertness: a single glassy carbon deposit and a double layer made of pyrocarbon deposit followed by a glassy carbon deposit. Molten salt and graphite were characterized after the thermal treatment using powder X-ray diffraction (PXRD), Scanning Electron Microscopy coupled with the Energy Dispersive X-ray spectrometry (SEM–EDX) and micro-Raman spectroscopy. This paper deals with detailed characterization of the molten salt interactions with the surface of four graphite samples: (i) raw graphite disc, (ii) graphite disc coated by glassy carbon obtained from the pyrolisis of a deposit of the phenolic resin precursor on an horizontal surface of graphite (named 'horizontal' coverage), (iii) graphite coated by glassy carbon obtained from the pyrolisis of a graphite discs dipped in phenolic resin precursor (named 'dip' coverage), (iv) graphite disc first covered by pyrocarbon and then by glassy carbon by horizontal coverage.

2. Experimental section

2.1. Preparation of the coatings of graphite

Graphite discs (10 mm diameter, 3 mm thickness), obtained from NBG-17 nuclear graphite, were prepared by SGL carbon group from graphite largest particles (800 μm) and pitch as binder.

* Corresponding author.
E-mail address: laurent.duclaux@univ-savoie.fr (L. Duclaux).

0022-3115/$ - see front matter © 2008 Elsevier B.V. All rights reserved.
doi:10.1016/j.jnucmat.2008.11.032

Nuclear graphite (apparent density: 1.85) shows a 7% porosity measured by mercury porosimetry with macropores (average diameter: 20 μm).

Two types of protection layers were prepared: glassy carbon and pyrocarbon/glassy carbon deposits. Glassy carbon coating was prepared from impregnation of phenolic resin (>500 mm) and then by carbonisation up to 1200 °C under inert atmosphere. Prior to impregnation, graphite discs were polished mechanically using SiC paper (400–4000 technical grade) in order to get a planar surface, and washed in distilled water under ultrasonic bath to clean the surface by removing the solid particles attached to the surface. The elaboration of glassy polymeric carbon was achieved by the carefully controlled carbonisation of a phenolic resin in an inert environment [4,5]. Phenol–formaldehyde resin (RESOL, Borden S.A.) was chosen as the organic precursor. After a curing step, the resin was pyrolized at low temperature rates to avoid disruptions and changing shape. The deposition of the resin on the graphite discs or rods has been performed by impregnation of a diluted solution of the resin in ethanol (25% v/v) allowing to decrease its viscosity and to get a thin layer (several 10 μm to several μm) of reticulated resin. Two kinds of impregnation procedures were performed: (1) The resin solution was dropped on the horizontal graphite disc (this kind of coverage is later named 'horizontal coverage'); (2) The graphite disc was dipped in the diluted resin, therefore covering the two faces and allowing a better control of the deposit thickness and homogeneity (this is the so-called 'dip' coverage).

Glassy carbon was prepared by the direct pyrolysis of the precursor in four steps. First, the resin was kept one night for degassing. The reticulation of the resin was achieved under air by heating from room temperature to 130 °C, at 6 °C/h. Next step was a post-reticulation until 230 °C, at 18 °C/h. At this step polycondensation reactions built a 3D network as the linear chains were cross linked. Then, the pre-carbonisation from ambient temperature to 600 °C, (heating rate of 2–10 °C/h), and the carbonisation to 1200 °C (heating rate of 40 °C/h) were performed in a quartz tube using a tubular furnace under nitrogen flow. The pre-carbonisation step has led to a conducting material due to the conjugation of the aromatic rings and hydrogen release. At 1200 °C, the structure and microtexture of glassy carbon well characterized by TEM, He pycnometry and XRD, were already achieved. The glassy carbon coating has shown densities ranging from 1.3 to 1.5 g/cm^3, significantly lower than graphite indicating a relative porosity of about 35%. Closed pores with nanometric size 5–10 nm were observed clearly on the TEM micrographs. A further heat treatment up to 2700 °C led to the shrinkage of entangled graphene ribbons observed by TEM concomitant to the increase of coherent domain sizes along *c* axis (Lc). Moreover, the XRD analysis has shown the absence of evolution of the (*10.*) and (*11.*) peaks of the carbon coatings in the range [1200 °C–2800 °C] consistent with a non-graphitising carbon. The XRD and TEM observations have confirmed that a glassy polymeric carbon structure was prepared. This structure is formed of an arrangement of randomly oriented graphene planes where the closed porosity appears in between the entangled graphene ribbons as reported by Jenkins et al. [6].

The deposits obtained by 'dip'-coating (i.e. by 'dip' coverage) show a quite good adhesion as compared to the horizontal ones but wide cracks are observed on the surface. However, due to shrinkage it appears quite difficult to cover at once a graphite cylinder rod by a uniform layer of glassy-like carbon. For a more homogenous and complete covering it is recommended to perform at least two impregnation/pyrolysis cycles successively. To overcome this tedious process, we have first deposited a film a pyrocarbon (0–10 μm) by the thermal decomposition of propylene diluted in nitrogen (10% v/v) at 800 °C for 30–60 min (Fig. 1(A)) and secondly impregnated the surface by phenolic resin following the pyrolisis steps previously described to obtain vitreous carbon. By filling the porosity of the graphite substrate, the pyrolitic carbon coating enables the formation of a smoother graphite surface on which a further impregnation of carbon precursor is achieved. The decrease of the shrinkage phenomenon is giving rise to a glassy carbon deposited on pyrocarbon with better homogeneity and adhesion (Fig. 1(C)). The following glassy carbon film presents thin cracks and small porosity (Fig. 1(B)).

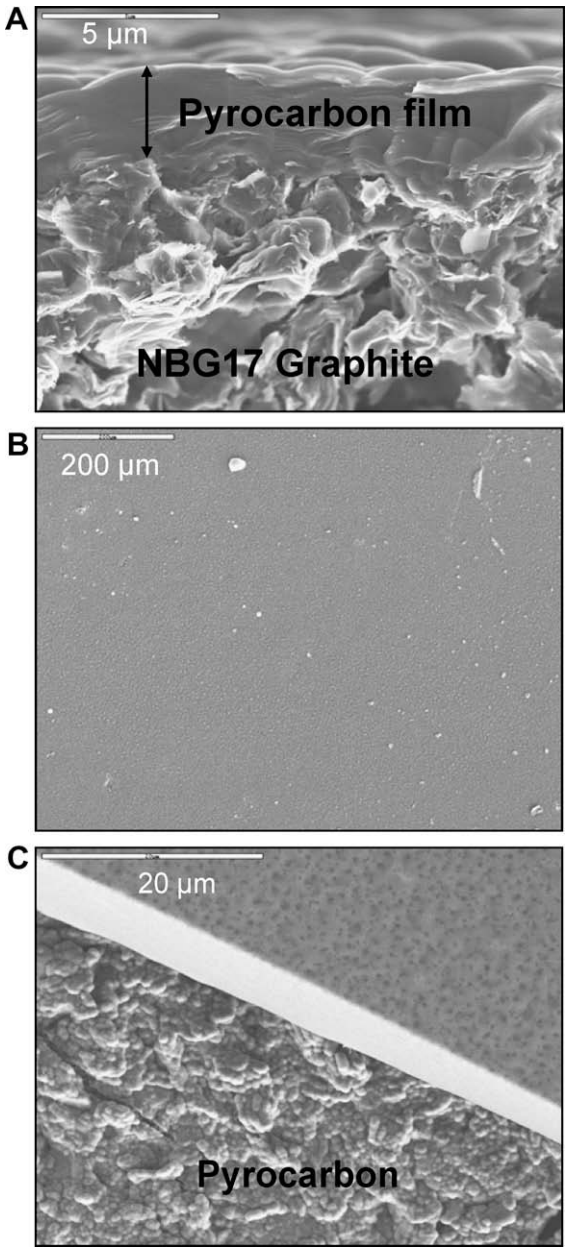

Fig. 1. SEM micrographs (secondary electrons) of: (A) the section of raw graphite disc coated by pyrocarbon film; (B) the surface of glassy carbon coating formed on the previous pyrocarbon deposit; (C) cross section showing the coating of glassy carbon on the pyrocarbon deposit.

2.2. Molten salt

Molten salt was synthesised from commercial LiF, NaF (greater than 99% purity; from Aldrich and Fluka, respectively) and ZrF_4 prepared in two steps. First, ZrO_2 (distributed by Merk) was attacked with boiling HF solution (40 wt%) and heated at 80 °C until

complete HF evaporation. Then, the obtained hydrated fluoride $ZrF_4 \cdot xH_2O$ was treated under pure fluorine gas flow at 500 °C for 24 h and yielded pure β-ZrF_4 powder. Commercial LiF and NaF were heated under vacuum prior to use. The purity of the obtained ZrF_4, NaF and LiF powders was confirmed by PXRD and ^{19}F MAS-NMR. The molar composition of the ternary eutectic fluoride salt corresponds to 27.0 mol.% LiF, 36.5 mol.% NaF and 36.5 mol.% ZrF_4 [7–8]. This composition, represented by the empty circle in the ternary diagram (ZrF_4–NaF–LiF) represented in Fig. 2, is a three phases domain composed of Li_2ZrF_6, Na_2ZrF_6 and $Na_7Zr_6F_{31}$. Representation of the ternary phase diagram in Fig. 2 was taken from the study of Thoma et al. [8] without taken into account the Li_4ZrF_8 phase [9,10]. PXRD analysis on the resulting cooled fluoride salt, after heating at 500 °C, showed the presence of these three phases. A melting temperature of 436 °C was determined for our synthesized fluoride salt by differential scanning calorimetry in good agreement with the literature: 425 °C [7] and 436 °C [8].

2.3. Immersion of graphite in molten salt/heat treatment

The eutectic molten salt loosed about 10% in weight (wt%) when heating during two days at 500 °C. This weight loss was attributed to a partial vaporization of the molten salt. The evolution of the heated molten salt composition (Table 3, Fig. 2) indicated that the vapour phase was mainly composed of sodium fluoride (NaF) and zirconium fluoride (ZrF_4). Literature indicates that for the studied composition and temperature range the vapour phase should be composed $NaZrF_5$ with small amounts of NaF and ZrF_4 [11]. Moreover we have brought out the presence of mainly the Na and F elements by EDX analyses of the solid deposit condensed at the exit of the furnace due to the evaporation of the heated molten salt. In order to avoid this weight loss during immersions of graphite discs in the molten salt at 500 °C, a nearly airtight reactor

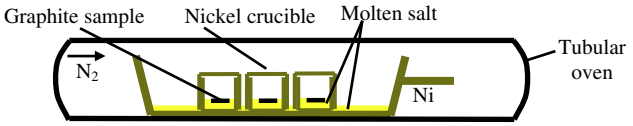

Fig. 3. Scheme of the device used for the airtight immersion of graphite in the molten salt.

was used (see Fig. 3). Before impregnation experiments of graphite by molten salt, the graphite discs were carefully washed in ethanol 15 min in an ultrasonic bath to avoid any contamination by dust particles and oven dried 8 h at 110 °C. The graphite disc and the fluoride salt were introduced in a closed (without welding) nickel crucible soaked in a secondary molten salt bath. This secondary molten salt bath prevented the evaporation inside the nickel crucible by maintaining a saturated vapour. Graphite discs and molten salt were introduced in these closed nickel crucibles and heated at 500 °C for 30 min, 48 h and 60 h under nitrogen flow in order to investigate the interactions between the surface disc and the fluoride molten salt. Experiments were also performed with graphite powder mixed with the molten salt in order to increase the graphite surface contact during the heat treatment.

2.4. Analyses

All samples were characterized by PXRD, micro-Raman spectroscopy and SEM–EDX before and after immersions.

2.4.1. PXRD analyses

X-ray powder patterns were recorded at room temperature using a Siemens D5000 diffractometer, Bragg-Brentano geometry, Cu K_α radiation ($\lambda = 1.54184$ Å), diffraction range $5° < 2\theta < 100°$, step size $\Delta 2\theta = 0.03°$ and a counting time of 2 s per step leading

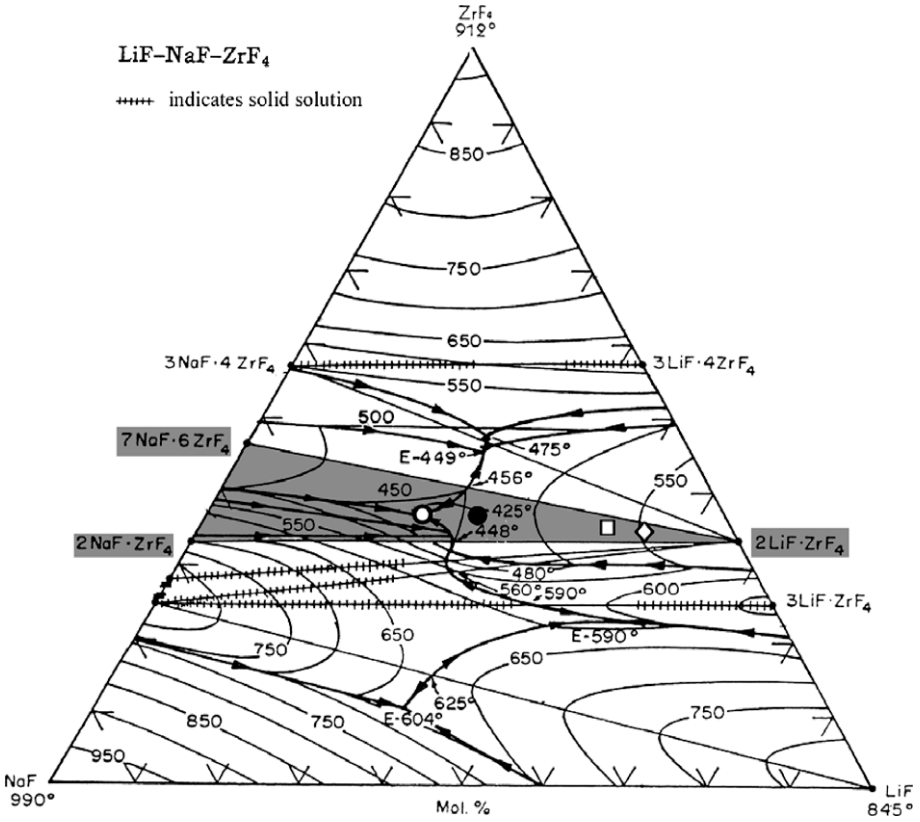

Fig. 2. Theoretical composition (○) of molten salt, and refined composition from semiquantitative Rietveld analyses before (●) and after immersion at the surface of the graphitic disc (□) and in the bulk molten salt (◊). Figure based on, drawn from Thoma et al. [8].

to a measuring time close to 2 h per sample. In order to determine the nature of the crystallised phases and their weight amounts, the XRD powder patterns were analyzed by the Rietveld refinement method using the program *FULLPROF* [12]. Structural description of Li_2ZrF_6 phase was taken from [13]: trigonal $P\bar{3}1m$ space group with $a = 4.9733$ Å, $c = 4.658$ Å and three crystallographic independent atomic positions (1 Li, 1 Zr and 1 F). Structural description of Na_2ZrF_6 phase was taken from [14]: monoclinic $P2_1/c$ space group with $a = 5.5562$ Å, $b = 5.4069$ Å, $c = 16.073$ Å, $\beta = 95.886(6)$ Å and nine crystallographic independent atomic positions (2 Na, 1 Zr and 6 F). Structural description of $Na_7Zr_6F_{31}$ phase was taken from [15]: rhombohedral $R\bar{3}$ space group with $a = 13.807$ Å, $c = 9.429$ Å and nine crystallographic independent atomic positions (2 Na, 1 Zr and 6 F). The graphite phase was also modelled when present according to [16]: hexagonal $P6_3/mmc$ space group, $a = 2.464$ Å, $c = 6.711$ Å and two crystallographic independent carbon positions. The diffraction peak profiles (both instrumental and intrinsic sample) were modelled by using a Thomson-Cox-Hasting pseudo-Voigt function [12]. The instrumental resolution function of the diffractometer has been previously determined by using pure silicon standard. The modellisation of the graphite phase was achieved (due to the highly anisotropic crystallite morphology) by introducing asymmetric parameters for the first (002) Bragg peak, anisotropic line broadening and preferential orientation. Fig. 4 shows the Rietveld refinement results on a graphite disc (Fig. 4(A)), on the as-prepared molten salt (Fig. 4(B)) and on sampling at the surface of a graphite disc impregnated with the molten salt (Fig. 4(C)).

2.4.2. Micro-Raman analyses

μ-Raman spectra were recorded at room temperature in the backscattering geometry using a Jobin-Yvon T64000 device spectrometer. The spectral resolution obtained with an excitation source at 514.5 nm (argon ion laser line, Spectra Physics 2017) is about 1 cm^{-1}. The Raman detector is a charge coupled device (CCD) multichannel detector cooled down to 140 K with liquid nitrogen. The laser beam was focused onto the sample through an Olympus confocal microscope with ×50 or ×100 magnification. Laser spot was about 1 μm^2. Measured power at the sample level was kept less than 15 mW in order to avoid any damage to the sample. The Raman scattered light was collected with the microscope objective at 180° from the excitation and filtered with an holographic Notch filter before being dispersed by a single grating (1800 grooves per mm). Several spectra were recorded (by accumulating three spectra of 60 s each) at different points for the same sample in order to evaluate the homogeneity of the samples and the reproducibility of the main spectral features. Spectra were recorded over the frequency range 300 cm^{-1}–3700 cm^{-1} in order to investigate the D (close to 1350 cm^{-1}), G (close to 1580 cm^{-1}), D' (close to 1620 cm^{-1}), 2D (close to 2700 cm^{-1}) and 2D' (close to 3250 cm^{-1}) bands characteristic of graphite samples [17]. Spectra were analysed by using the profile fitting procedure with a Lorentzian function of the program *SPECTRAW* [18]. Several graphitization indices can be deduced from frequency of the G band, the line widths of the G and 2D bands, and the integrated intensity ratio $R = I_D/I_G$ (inversely proportional to the graphitisation level) [19]. I_D is the integrated intensity of the D band (relative to the induced

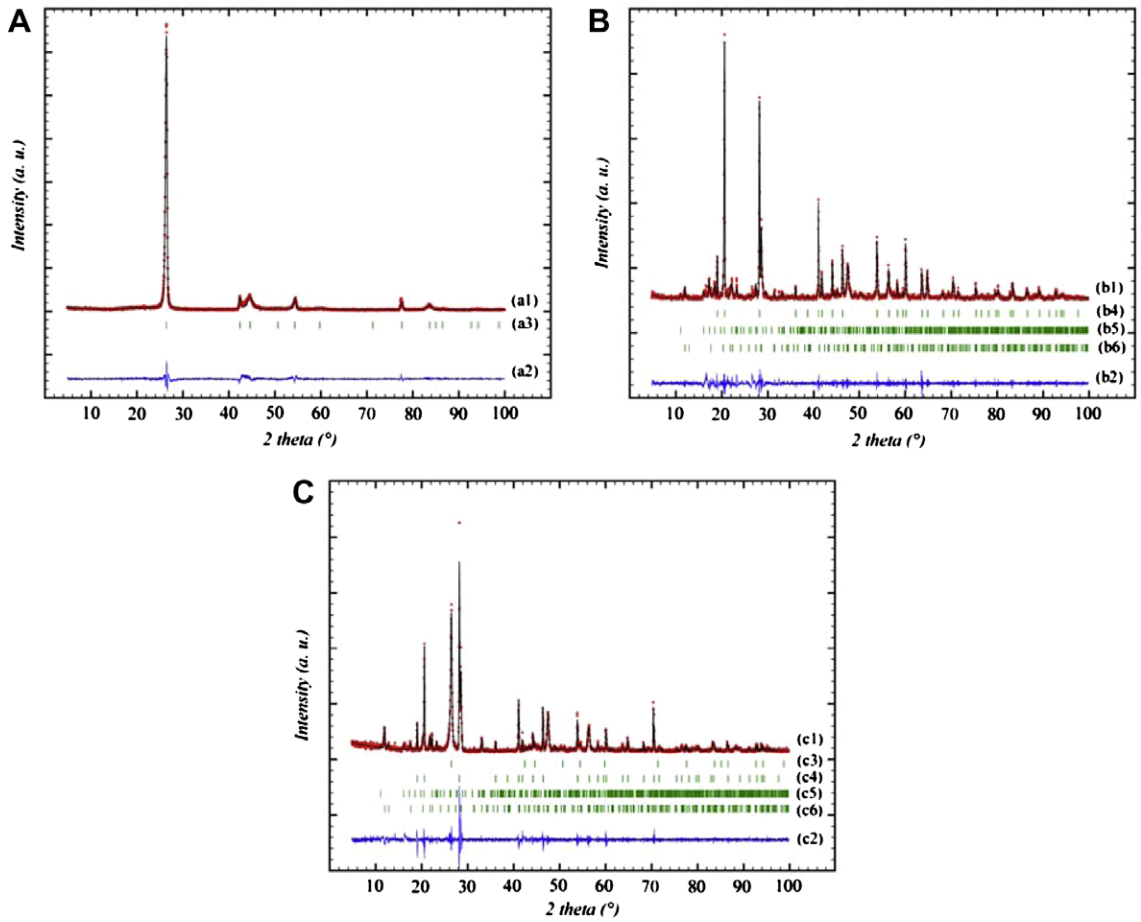

Fig. 4. Rietveld plots of the graphite disc (A), the fluoride molten salt (B) and the graphitic surface impregnated by the molten salt (C). Observed (dots) and calculated (solid lines) powder patterns (a1, b1 and c1; $\lambda = 1.5418$ Å) are shown with difference curves (a2, b2 and c2). The ticks indicate the Bragg peak positions of graphite (a3 and c3), Li_2ZrF_6 (b4 and c4), Na_2ZrF_6 (b5 and c5) and $Na_7Zr_6F_{31}$ (b6 and c6).

Table 1
Raman and PXRD parameters of the raw graphitic discs before immersion in the molten salt.

Raman analysis					PXRD
Spectrum (magnification)	Band frequency (cm^{-1})			$R = I_D/I_G$	d_{002} (Å)
	D	D'	G		
No. 1 (×100)	1355	–	1581	0.26	3.377
No. 2 (×50)	1354	1623	1581	0.42	
No. 3 (×100)	1355	1622	1581	0.48	
No. 4 (×100)	1354	1623	1582	0.50	
No. 5 (×100)	1355	1623	1583	0.59	

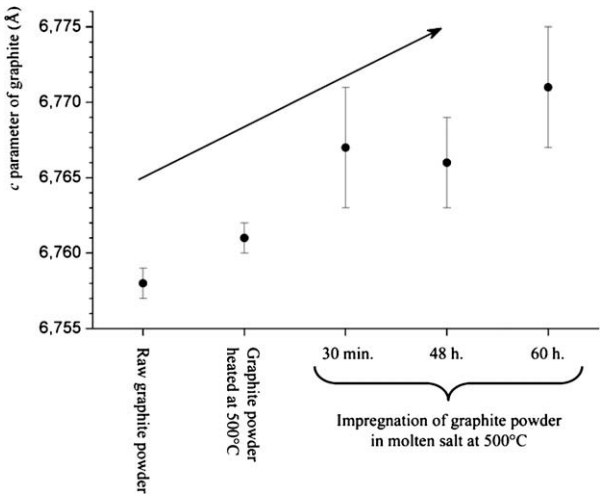

Fig. 5. Evolution of the *c* lattice parameter of graphite powder after heat treatment and immersion in molten salt at 500 °C.

graphite disorder) and I_G the integrated intensity of the G band (the E_{2g} band, relative to the well crystallised graphite).

2.4.3. SEM–EDX analyses

The samples were studied by SEM with a stereoscan 440 microscope (Leica) coupled with a Kevex Sigma X-ray spectrometer. The interactions between graphite and molten salt were observed by secondary electrons and by backscattered electrons to analyse the surface topography and the distribution of salt particles on graphite, respectively. X-ray microanalysis was performed to compare the qualitative elemental composition of salt phases and to observe possible graphite intercalation compounds. Moreover, to get information on the penetration of salt into the graphite, the samples were analyzed from outside toward inside the graphite disc according to a cross section. Before SEM observations, these samples were impregnated in resin (epofix resin, cat no. 40200029, distributed by Struers) under vacuum, polished with 400–4000 grit silicon carbide papers in ethanol, washed in a ultrasonic bath (to avoid pollution from polishing) and metallized (with carbon, 10 nm thickness). Samples were analysed by SEM–EDS before the impregnation in molten salt to check the cleanliness of the surface discs.

3. Results and discussion

3.1. Characterizations of materials before the high temperature impregnations

A characterization of the used fluoride salt and graphite discs was realized in order to investigate subsequently their interactions at the surface of the graphite disc. The ratio $R = I_D/I_G$ was determined from Raman spectra, and the interplanar distance, d_{002}, was determined by Rietveld refinement on PXRD patterns. Table 1 indicates the frequencies of the D, D' and G bands, and the *R* ratio measured from different spectra recorded on the same graphite disc (and using either ×50 or ×100 magnification for the focalisation). Theses analyses highlighted the heterogeneity of the used raw graphite discs; a variation of the *R* ratio (from 0.26 to 0.59) was observed for the same graphite disc. The raw graphite disc is heterogeneous at the micron scale, and exhibits an important disorder. Raman spectra confirm that nuclear graphite is made of graphite particles combined with a highly disordered carbon due to the graphitization of the pitch binder. PXRD pattern indicated that the crystallized part of the disc perfectly corresponds to graphite (Fig. 4(A)) with the following refined lattice parameters: $a = 2.4610$ (2) Å and $c = 6.755$ (1) Å for the graphite disc, and $a = 2.4625$ (2) Å and $c = 6.758$ (1) Å for the graphite powder.

3.2. The graphite–molten salt interactions after the high temperature impregnations

3.2.1. XRD analyses

Graphite characterization. Graphite discs without protection and coated with the three kinds of protection layers have been analyzed by PXRD after the impregnation (30 min, 48 h and 60 h). PXRD patterns of the graphite discs surface show the presence of graphite and as well as the three fluorinated phases from the molten salt. Fig. 4(C) shows the Rietveld refinement result from PXRD pattern recorded on an impregnated graphite disc.

Fig. 5 displays the evolution of the *c* lattice parameter of the graphite powder after the impregnations with molten salt as a function of the heating time. A simple heat treatment of graphite disc at 500 °C for 48 h in nitrogen atmosphere results in a weak increase of the *c* lattice parameter, from 6.758 (1) Å to 6.761 (1) Å, indicating that such a heat treatment induces a weak disorder of the graphite layer stacking. Impregnations in the molten salt at the same temperature (500 °C) led to a more pronounced increase of the *c* lattice parameter. Moreover the increase of the *c* lattice parameter was time dependent, from 6.767 (4) Å after half an hour of impregnation to 6.771 (4) Å after 60 h of impregnation. The presence of the fluoride molten salt at 500 °C increases the graphite stacking disorder observed at the disc surface. However, the observed evolution of the *c* lattice parameter of graphite (about

Table 2
Variation of the *c* lattice parameter of graphite coated with protection layer during heat treatment (500 °C, 2 days). (*h.c.*: horizontal coverage, *d.c.*: 'dip' coverage).

		c Parameter (Å)		Adherence
		Value before impregnation	Variation after impregnation	
Powder of graphite		6.758	0.013	–
Raw graphitic disc		6.755	0.013	Strong
Graphitic disc coverage	Glassy carbon (*h.c.*)	6.742	0.010	Very strong
	Glassy carbon (*d.c.*)	6.764	0.005	Medium
	Pyrocarbon followed by glassy carbon (*h.c.*)	6.750	0.003	Weak
	Pyrocarbon followed by glassy carbon (*d.c.*)	6.759	−0.011	Very weak

0.013 Å) is too weak to allow the intercalation of elements from the molten salt into the graphite stacking.

Table 2 denotes the variation of the *c* parameter and the adherence (which was qualitatively classified in categories, from very strong to very weak, by the strength necessary to remove the molten salt rind from the surface of the graphite disc) after 2 days of contact with the molten salt at 500 °C (raw and protected discs). The raw graphite materials (either disc or powder) display the highest increase of the *c* lattice parameter: 0.013 Å. Protection coating (by a simple glassy carbon deposit or a double pyrocarbon deposit followed by a glassy carbon deposit) allows to reduce the variation of the graphite *c* lattice parameter. When the protection is made by a pyrocarbon deposit followed by 'dip' glassy carbon coverage a decrease of the *c* lattice parameter is observed. From these *c* lattice parameter variations it can be deduced that 'dip' coverage induces a better protection of the graphite disc than horizontal coverage. Moreover, the adherence of the molten salt on the graphite disc surface can be correlated with the variation of the graphite *c* lattice parameter. A strong variation of the *c* value corresponds to a greater adherence (cases of raw graphite disc and

Table 3
Refined compositions (from semi-quantitative Rietveld refinements) of the molten salt before and after impregnation. Compositions obtained for the molten salt after impregnation correspond to averaged values (from four different samplings). Symbols (○, ●, □, ◊) are related to Fig. 2.

	Molten salt composition				
	Before impregnation			After 48 h of impregnation at 500 °C	
	Theoretical (○)	Heated at 500 °C		At the graphite disc surface (□)	In the bulk molten salt (◊)
		30 min	48 h (●)		
Li_2ZrF_6 (wt%)	35.5	47	51	70	77
Na_2ZrF_6 (wt%)	35.0	36	34	18	15
$Na_7Zr_6F_{31}$ (wt%)	29.5	17	15	12	8
LiF (wt%)	8.4	11	12	17	18
NaF (wt%)	18.4	16	15	9	7
ZrF_4 (wt%)	73.2	73	73	74	75
LiF (mol.%)	27.0	34	37	49	54
NaF (mol.%)	36.5	30	28	16	12
ZrF_4 (mol.%)	36.5	35	35	35	34

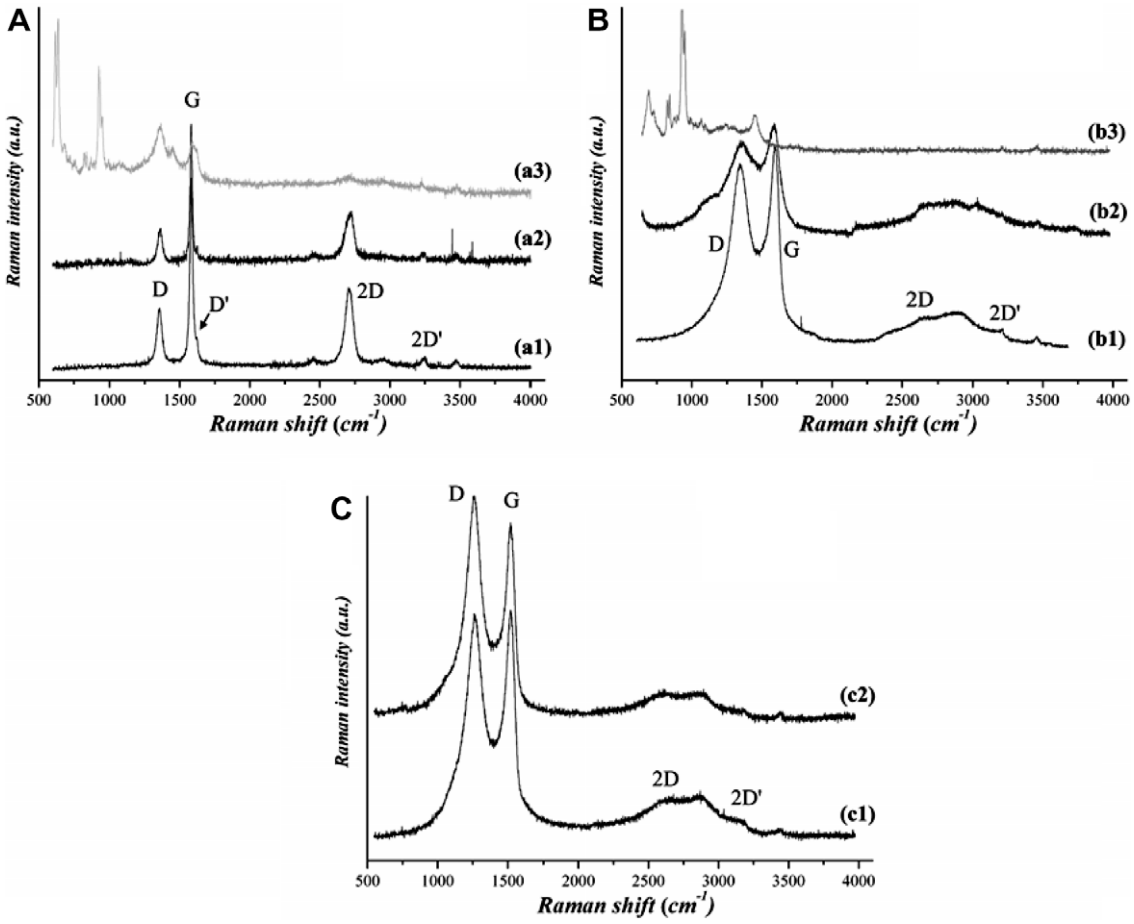

Fig. 6. Raman spectra recorded at the disc surfaces of raw graphite (A), graphite coated by a glassy carbon layer (B) and graphite protected by a double layer of pyrocarbon and glassy carbon (C). Spectra recorded before impregnation (a1, b1 and c1) and after impregnations (a2, b2 and c2). Spectra a3 and b3 obtained from the fluoride molten salt after impregnation at 500 °C for 48 h.

graphite disc coated by a horizontal coverage of glassy carbon; see Table 2), and a weak variation or a decrease of the *c* value may be related to a weak adherence (cases of the pyrocarbon deposit followed by glassy carbon coverage). Then the induced graphite disorder and the resulting strength of adherence are correlated.

Molten salt characterization. The evolution of the phase composition of the molten salt during the impregnation was characterized by comparing the semi-quantitative Rietveld analyses before and after impregnations. The refined phases composition (in wt%), with the corresponding elementary fluorides composition (wt% and mol.%), are gathered in Table 3 together with the theoretical eutectic composition. The refined amounts of the observed phases were relatively far from the theoretical values, namely after but already before the impregnation (see Fig. 2). Although the divergence from the theoretical values is marked by considering directly the refined weight phases amounts (about 12 wt% excess of Li_2ZrF_6 compensated by an underestimation of $Na_7Zr_6F_{31}$ before impregnation), it becomes really fair when considering the corresponding elementary fluorides weight percents (about 3 wt% excess of LiF and 3 wt% missing of NaF). The refined weight percent of ZrF_4 (Table 3) was closed to the initial theoretical value (between 73 and 75 wt%, compared with the 73.2 theoretical value). The deficiency in NaF, which is compensated by the excess in LiF, can be due to an underestimation of the $Na_7Zr_6F_{31}$ phase combined with an overestimation of the Li_2ZrF_6 phase. This may be due to a poorly crystalline $Na_7Zr_6F_{31}$ phase and the possible Na insertion in the Li_2ZrF_6 phase. Although such a solid solution was not mentioned in the literature [7,8], it occurs in analogous Th phases $(Na,Li)_7Th_6F_{31}$ [20]. This observed divergence was increased when analysing the molten salt after impregnation with graphite.

If only NaF vapour loss would appear during impregnation heat treatment, thus both ZrF_4 and LiF weight percents might have been increased. As the observed ZrF_4 wt% (Table 3) after 48 h of salt heat treatment (at 500 °C) is slightly decreased compared with the initial ZrF_4 wt% in the eutectic salt (35 compared with 36.5 wt% initial value); the weight loss of ZrF_4 is achieved during heat treatment of the molten salt. The weak variation of the graphite *c* lattice parameter is consistent with the non intercalation of Na into graphite. The several obtained compositions are represented in the ternary diagram (Fig. 2) by assuming that no amorphous phases and no solid solution appeared when cooling the molten salt. Fig. 2 shows that discrepancy is mainly due to a loss of sodium and zirconium fluorides probably in form of vapour (leading to an underestimation of the $Na_7Zr_6F_{31}$ phase and an overestimation of the Li_2ZrF_6 phase). On the assumption that LiF is not vaporized during heat treatment at 500 °C, the excess of LiF weight% (Table 3) after heating the salt, can be the signature of the enrichment in LiF of the final composition to compensate the loss of NaF and ZrF_4. Assuming that LiF is absent in the vapour compounds, the composition of vapour evolving from the bulk molten salt, calculated from Table 3 in case of 48 h heat treatment at 500 °C (by difference of the salt molar compositions before and after annealing) is $\sim 0.6[NaF] + 0.4[ZrF_4]$ (i.e. $Na_3Zr_2F_{11}$). This vapour phase composition can be written in the form of $2[NaZrF_5] + NaF$, where $NaZrF_5$ is a compound which was previously detected by Sense et al. in the vapour phase evolving from the NaF–ZrF4 system [11]. Moreover, the additional NaF vapour missing correlates well with the Na and F elements EDX observations, made on the solid collected by condensation of vapour (on glass plate at the end of the tubular furnace) from the used molten fluoride salt at 500 °C. With the

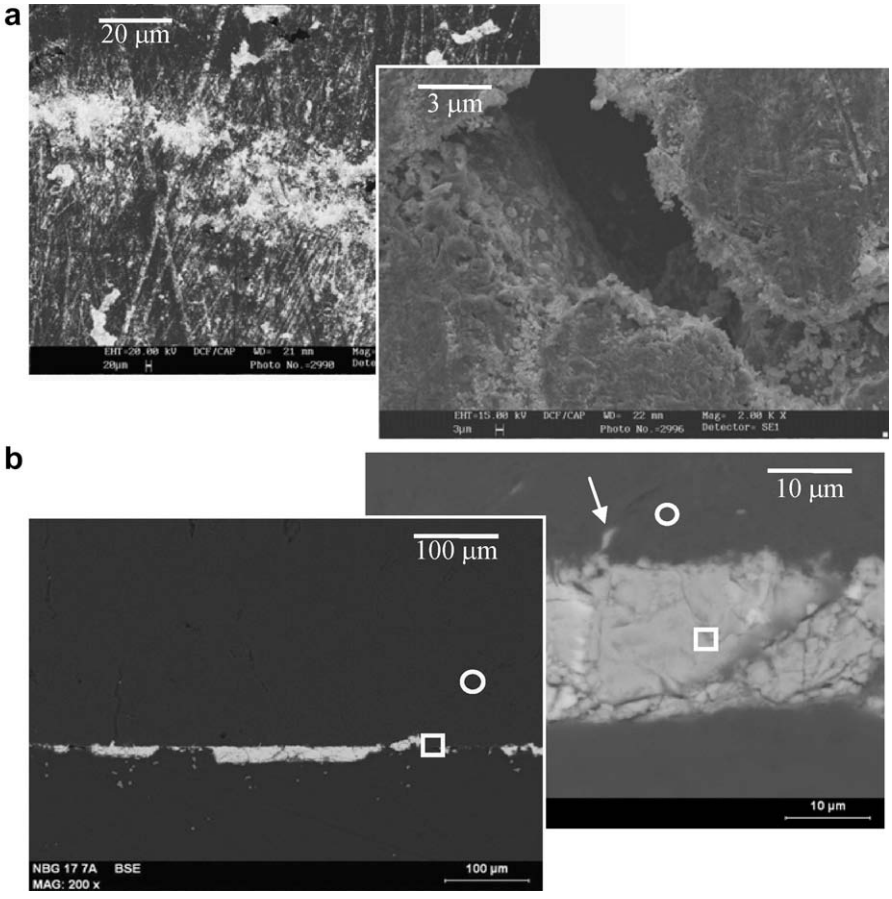

Fig. 7. SEM micrographs on the backscattered electrons mode of the raw graphite disks after their immersion in molten salt (500 °C, 48 h): (a) disc surface; (b) cross section. The graphite disks are indicated by empty circle (○). The salt films covering the graphite surface are indicated by empty square (□). The arrow displays a zone where the salt has entered the porosity (the penetration depth of the graphitic disc is less than 4 µm).

same hypothesis that LiF is a non volatile compound, the composition of gas phase can be estimated from Table 3, in case of impregnation of graphite by examining the difference of salt composition (molar) before and after 48 h heat treatment at 500 °C. Thus, the calculated composition of the vapour evolving from the bulk molten salt or salt at the disc surface, is also equal to $2[NaZrF_5] + NaF$. This confirms that the composition of the vapour phase in equilibrium with molten salt at 500 °C in contact or not with graphite discs is $2[NaZrF_5] + NaF$. The difference in molar compositions (Table 3 and fig. 2) observed between the bulk salt and the salt impregnating the graphite disc, is only due to an increase of the weight loss of the gas phase compound. Nevertheless phases composition of the cooled salt always corresponds to the three phases domain Li_2ZrF_6–Na_2ZrF_6–$Na_7Zr_6F_{31}$.

3.2.2. Raman analyses

Raman spectra recorded at the graphite disc surface before and after impregnation are shown in Fig. 6 for raw graphite disc without protection (Fig. 6(A)), graphite disc protected by a glassy carbon coating (Fig. 6(B)), and graphite disc first covered by pyrocarbon and then by glassy carbon layer (Fig. 6(C)).

Disc of raw graphite. Spectra recorded before and after the impregnation (Fig. 6(A)) show the expected D, G, D', 2D and 2D' bands of graphite [16] with roughly the same intensities ratios. Due to the heterogeneous presence of highly disordered carbon as pitch binder in the raw graphite disc, the observations about the characteristic ratio $R = I_D/I_G$ [19] from Raman spectra were difficult to interpret. Nevertheless a broadening of the 2D band was evidenced indicating an increase of the graphite disorder at the disc surface [19]. Raman analyses performed on the molten salt after impregnation reveals the presence of highly disordered carbon particles, coming from the unprotected graphite disc, in the molten salt.

Disc of graphite covered by the protection layers. Spectra were recorded at the surface of graphite discs covered by a glassy carbon layer (Fig. 6(B)) and a pyrocarbon deposit followed by a glassy carbon layer (Fig. 6(C)). Spectra recorded before impregnation shows a large $R = I_D/I_G$ ratio (superior to 1), and an important broadening of the 2D and 2D' bands, confirming the presence of a highly amorphous carbon layer at the graphite disc surface. Spectra again highlight an increase of the graphite disorder after the salt immersion of the covered discs. Fig. 6(B) (case of the simple glassy carbon layer protection) shows an important broadening of the D band. Finally Fig. 6(C) (case of the double layer of pyrocarbon and glassy carbon) shows a slight increase of the I_D/I_G value (slight increase of the D band intensity compared to the G band). Raman spectra from the molten salt after the impregnations did present neither the D nor the G bands indicating the absence of extracted graphite particles in the molten salt and a better behaviour of the protected graphite discs in the presence of the fluoride molten salt at 500 °C (which can be correlated with the decrease of the molten salt adherence at the surface of protected graphite discs). In agreement with the PXRD results, Raman study confirms that the salt immersion has induced a slight increase the carbon disorder. By these Raman analyses the double pyrocarbon/glassy carbon coating appears as the more efficient protection since weak modifications of the D and G bands and no evidence of extracted graphite particles in the molten salt are observed after the immersion.

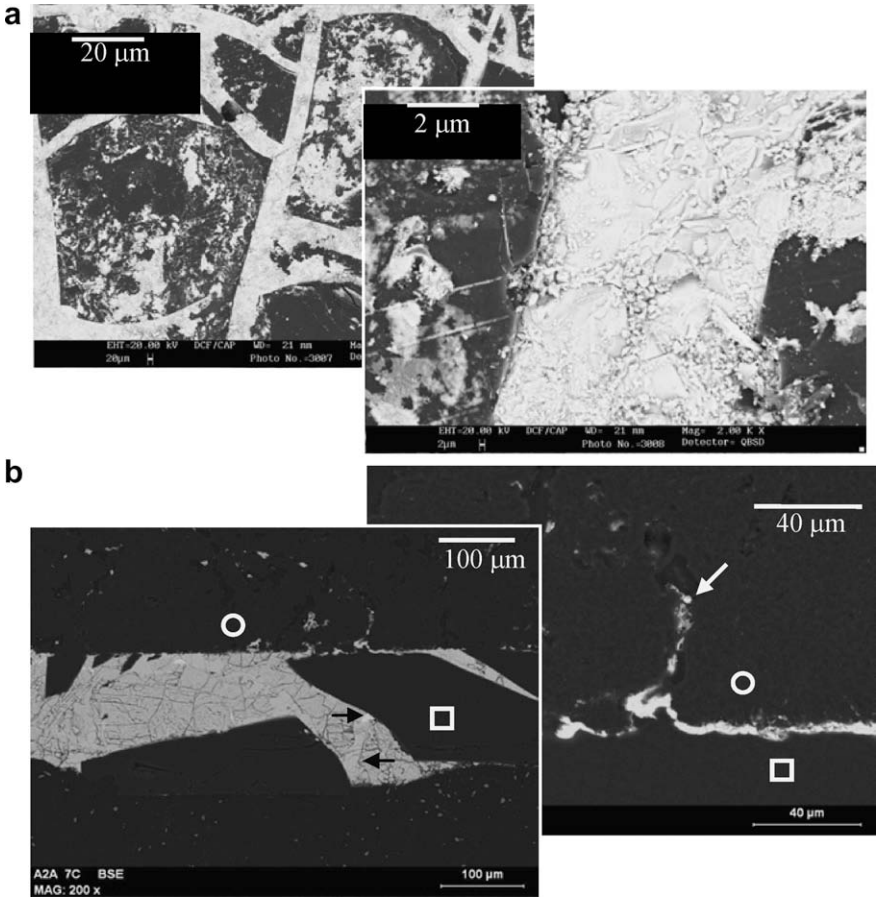

Fig. 8. Backscattered electrons SEM micrographs of graphite disc (○) coated with glassy carbon (□) (horizontal coat) after immersion in molten salt (500 °C, 48 h): (a) discs surface, (b) cross section. The white arrow displays the penetration of the salt in the graphite porosity. The black arrows show the limit of a white domain with lower F/Zr and Na/Zr atomic ratios.

3.2.3. SEM–EDX analyses

The surface disc porosity, the cohesion of the deposit protective layer, the adherence of the molten salt at the disc surface were studied by SEM secondary electrons images and backscattered electron images. Images were realized at the surface and on cross sections of the samples obtained from raw graphite disc (Fig. 7), from disc protected by horizontal glassy carbon coating (Fig. 8), or by 'dip' glassy carbon coating (Fig. 9), and from disc protected by the double coating pyrocarbon/glassy carbon (Fig. 10). X-ray microanalyses have shown the presence of F, Na and Zr elements in the fluoride phases at the surface of the discs. EDX analyses displayed the absence of coexistence of elemental carbon with the chemical elements of the salts. This means that in agreement with previous PXRD results, no graphite intercalation reaction was observed whatever the sample (unprotected graphite disc and the different protected graphite discs).

Disc of raw graphite. Raw graphite disc SEM images show a rough surface and a wide porosity in agreement with the mercury porosimetry characterization. SEM images showed the presence of salt particles, penetrating through the surface porosity of the graphite disc after an impregnation at 500 °C for 2 days (Fig. 7). This observation may be related with the strong adherence of molten salt obtained at the surface disc of raw graphite (as indicated in Table 2). Nevertheless, the pores were not completely filled and the penetration deepness of the graphite disc was less than 4 μm (Fig. 7).

Disc protected by horizontal glassy carbon coating. The horizontal coverage of glassy carbon is characterized by several wide cracks (of about 6 μm) but do not show any other porosity (Fig. 8). The cross section images reveal a thick deposit of glassy carbon (>150 μm) at the graphite surface. After the impregnation, the numerous glassy carbon cracks were completely filled with the molten salt. These fully impregnated cracks yields the very strong adherence observed for the horizontal glassy carbon deposit (Table 2). However the smooth surfaces of the glassy carbon domains were slightly impregnated by molten salt. A benefit effect of a regular glassy carbon layer (i.e. without cracks) seems to be obtained due to a very low adherence of the molten salt to the glassy carbon surface. Images from the cross section (Fig. 8(b)) showed the disastrous effect of the cracks. During impregnation the fluoride molten salt penetrated the cracks and was inserted between the graphite surface and the glassy carbon deposit. Thus the horizontal coverage is absolutely inefficient, and the salt has penetrated into graphite porosity up to 60 μm deep (Fig. 8). As a result, coating by single horizontal glassy carbon does not protect the nuclear graphite because of the very low adherence of the deposit.

Backscattered electrons images highlight two different domains: mainly grey areas and some rare white zones (Fig. 8) corresponding to different compositions of the molten salt. X-ray microanalyses performed on both white and grey domains have shown that in white area, F/Zr and Na/Zr atomic ratios are lower than in grey area. In fact, some phases of the salt possess lower amount of Na and F (white areas). These results are in agreement with the PXRD Rietveld refinements showing a loss of NaF from the molten salt during the heat treatment (Table 3 and Fig. 2).

Disc protected by 'dip' glassy carbon coating. The 'dip' coating of the phenolic resin precursor enables to prepare after pyrolisis a thin film of glassy carbon (3 μm thickness) which presents small cracks (3 μm broadness) and small pores (1 μm); as observed in Fig. 9. Molten salt penetrated the cracks and the porosity of the glassy carbon surface. The medium adherence observed (Table 2) is explained by the fineness of the deposit imperfections, and by a good cohesion of the deposit at the graphite surface. Molten salt has not deeply penetrated the porosity (<10 μm) (Fig. 9). The

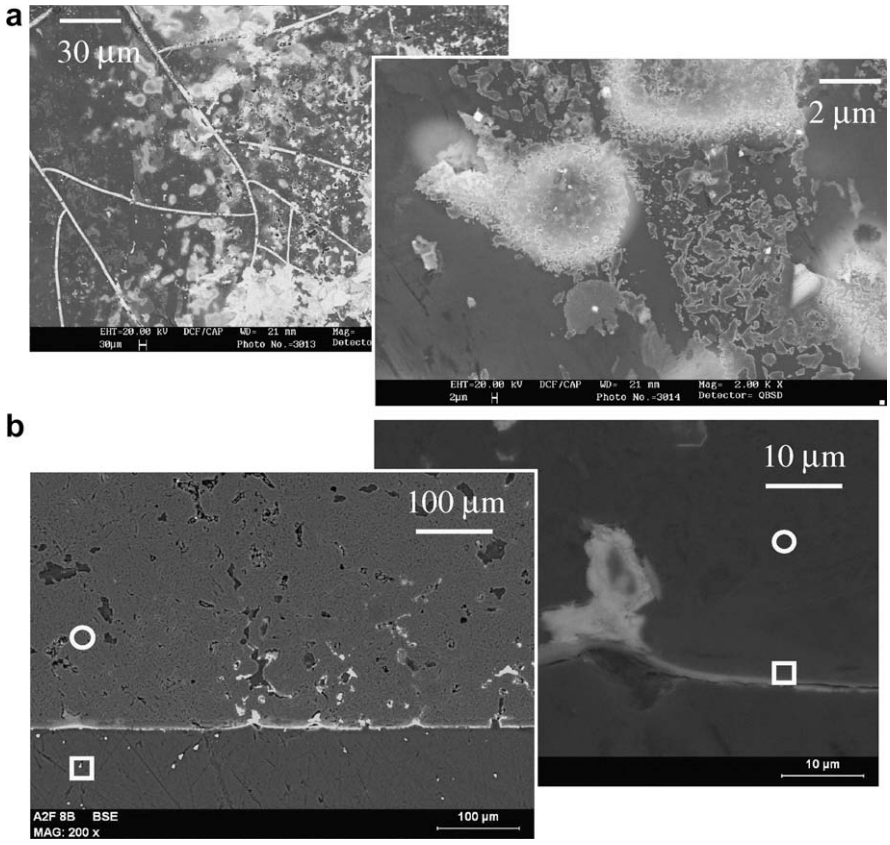

Fig. 9. Backscattered electrons SEM micrographs of graphite disc (○) coated with glassy carbon (□) ('dip' coat), after immersion in molten salt (500 °C, 48 h): (a) discs surface; (b) cross section.

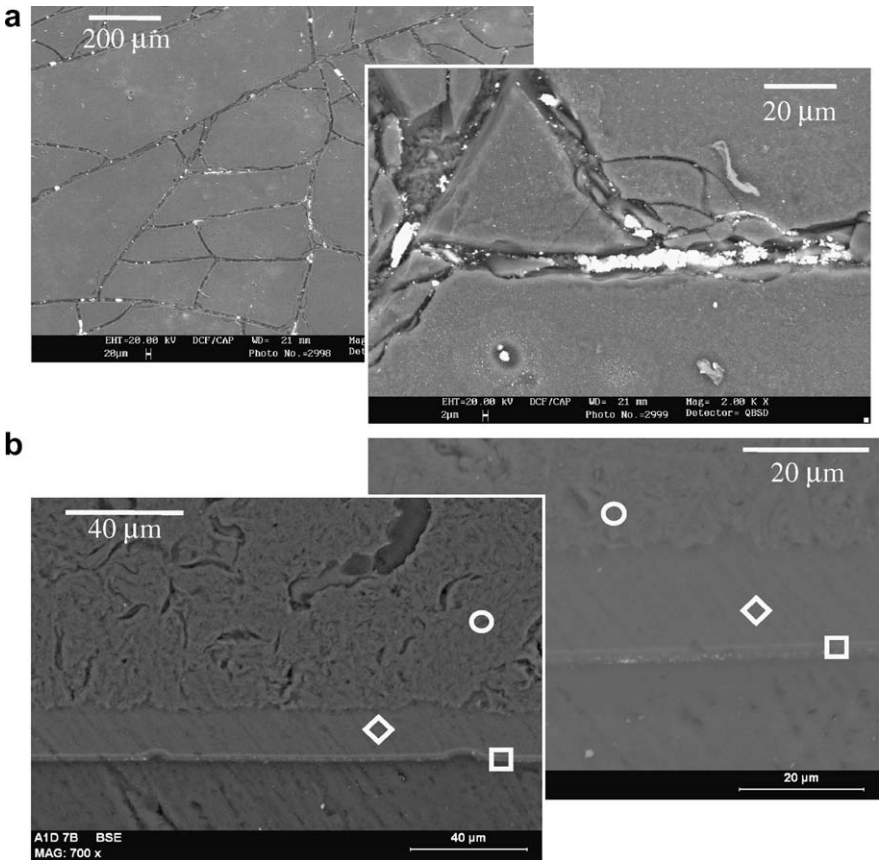

Fig. 10. Backscattered electrons SEM micrographs of graphite disc (○) coated with pyrocarbon (◇) and then with glassy carbon (□) (horizontal coat), after immersion in molten salt (500 °C, 48 h): (a) discs surface; (b) cross section.

adhesion of the glassy carbon is lower than in the sample prepared by horizontal coating, so the molten salt cannot diffuse at the glassy carbon and the graphite interface. This means 'dip' coating allows obtaining a better protection of graphite than the horizontal one.

Disc protected by the double pyrocarbon/glassy carbon deposit. Cross section analysis shows a thick coating of pyrocarbon (30 µm) covered by a thin film of glassy carbon (5 µm) (Fig. 10). Pyrocarbon fills porosity of graphite and allows a good adhesion of glassy carbon. The surface of glassy carbon exhibits a few cracks (~5 µm) and mainly small pores (0.5 µm) on an homogeneous zone of the deposit.

Very weak amount of molten salt is observed on the glassy carbon surface and in the cracks, in correlation with the observed weak adherence of the salt on this substrate (Table 2). The molten salt did not fill the pores as only very small and dispersed salt particles were fixed on the glassy carbon surface, and no diffusion through the double protection layer was observed (Fig. 10). The molten salt did not reach the nuclear graphite surface during impregnation. An efficient protection of the nuclear graphite towards the molten salt diffusion and a possible corrosion has been obtained by successive coating of pyrocarbon and glassy carbon.

4. Conclusion

As expected from the published ternary phases diagrams [7,8], our synthesized molten salt eutectic composition (27.0 mol.% LiF, 36.5 mol.% NaF and 36.5 mol.% ZrF_4) consists of the three phases Li_2ZrF_6, Na_2ZrF_6 and $Na_7Zr_6F_{31}$. Qualitative Rietveld refinements of cooled molten salts (after 48 h at 500 °C) show the fluoride salt lying in the three phases domain and semi-quantitative Rietveld analyses indicate the mean following phase amounts (73.5.5 wt% Li_2ZrF_6, 16.5 wt% Na_2ZrF_6 and 10.0 wt% $Na_7Zr_6F_{31}$) in spite of the pristine phase amounts (35.5 wt% Li_2ZrF_6, 35.0 wt% Na_2ZrF_6 and 29.5 wt% $Na_7Zr_6F_{31}$). This change in composition corresponds to the evaporation of a phase composed mainly of $NaZrF_5$ compound (as reported by previous authors [11]) and NaF from the eutectic molten salt heated at 500 °C. The exact composition of the gas phase evolving from molten salt at 500 °C, calculated from the semi-quantitative Rietveld analyses on the assumption that LiF is non volatile is $2[NaZrF_5]$ + NaF. The stoichiometry of this gas phase is not modified by impregnation of graphite materials in molten salt (at T = 500 °C) in inert atmosphere. This latter result and the X-ray microanalysis (using EDX) point out the absence of reactivity of graphite materials by with this eutectic molten salt for contact time of less than 48 h. The presence of Na and F elements in the residual deposit obtained from condensation of the vapour phase and the loss of these elements from salt domains were brought out by EDX analyses.

Impregnation of raw nuclear graphite disc in the molten salt for 48 h at 500 °C points out an evolution of the graphite surface, i.e. increase of the graphite stacking disorder (observed by a weak increase of the c lattice parameter and increase of the Raman D band), strong adherence of the cooled salt at the surface of the disc (with fluoride salt penetration in the graphite surface porosity observed by SEM), and some highly disordered graphite particle coming of the surface disc and dispersed into the molten salt. The surface of the nuclear graphite can be coated with different glassy carbon protection layers made from phenol–formaldehyde resin precursor before the molten salts impregnation. The analysis by SEM, Raman and X-ray diffraction of the protected graphite discs impregnated by molten salt (at 500 °C for 2 days) has allowed

checking the efficiency of the protection layer. A simple glassy carbon layer only brings out a slight improvement of the behaviour of the surface disc at the contact with molten salt. On the other hand, a double protection layer composed by a pyrocarbon and a subsequent glassy carbon deposit results in a good protection of the disc. This compact, and quite impermeable to the molten salt protection layer exhibits a perfect adhesion on the nuclear graphite surface and shows a very weak adherence towards the molten salt.

Acknowledgements

The authors thank Mr B. Tahon, (SGL Carbon, Cheddes, 74, France) for kindly providing the nuclear graphite samples. The authors thank the 'CNRS' (National Scientific Research Center) for its financial support through the 'molten salt research program' ('PCR Sels Fondus').

References

[1] L. Mathieu, D. Heuer, R. Brissot, C. Garzenne, C. Le Brun, D. Lecarpentier, E. Liatard, J.-M. Loiseaux, O. Méplan, E. Merle-Lucotte, A. Nuttin, E. Walle, J. Wilson, Progr. Nucl. Energy 48 (7) (2006) 664.
[2] J. Uhlir, J. Nucl. Mater. 360 (2007) 6.
[3] U. Gat, J.R. Engel, Nucl. Eng. Des. 201 (2000) 327.
[4] L.L. Korb, P.A. Waitkus, Vitreous carbon and process for preparation thereof, US Patent 4550,015, 29 October 1985.
[5] H. Maleki, L.R. Holland, G.M. Jenkins, R.L. Zimmerman, Carbon 35 (2) (1997) 227.
[6] G.M. Jenkins, K. Kawamura, Polymeric Carbons, Carbon Fiber, Glass and Char, Cambridge University Press, Cambridge, 1976.
[7] F.F. Blankenship, H.A. Friedman, R.E. Thoma, W.R. Grimes, in: R.E. Thoma (Ed.), Phase Diagrams of Nuclear Reactor Materials, Oak Ridge National Laboratory, ORNL-2548, 1959, p. 61.
[8] R.E. Thoma, H. Insley, H.A. Friedman, G.M. Hebert, J. Chem. Eng. Data 10 (3) (1965) 219.
[9] P. Dugat, M. El-Ghozzi, J. Metin, D. Avignant, J. Solid State Chem. 120 (1995) 187.
[10] O. Benes, R.J.M. Konings, J. Alloys Compd. 452 (2008) 110.
[11] K.A. Sense, C.A. Alexander, R.E. Bowman, R.B. Filbert, J. Phys. Chem. 61 (1957) 337.
[12] J. Rodriguez-Carvajal, PROGRAM FullProf.2k – version 3.30, Laboratoire Léon Brillouin (CEA-CNRS), France, 2005.
[13] G. Brunton, Acta Crystallogr. B 29 (1973) 2294.
[14] G. Brunton, Acta Crystallogr. B 25 (1969) 2164.
[15] J.H. Burns, R.D. Ellison, H.A. Levy, Acta Crystallogr. B 24 (1968) 230.
[16] P. Trucano, R. Chen, Nature 258 (1975) 136.
[17] S. Reich, C. Thomsen, Philos. Trans. Roy. Soc. A 362 (2004) 2271;
See also R.J. Nemanich, S.A. Solin, Phys. Rev. B 20 (2) (1979) 392;
See also F. Tuinstra, J.L. Koenig, J. Chem. Phys. 53 (3) (1970) 1126.
[18] D. Lovy, PROGRAM "Spectraw", Département de Chimie Physique, Université de Genève, 1996.
[19] P. Lespade, A. Marchand, M. Couzi, F. Cruege, Carbon 22 (4/5) (1984) 375;
See also P. Lespade, R. Al-Jishi, M.S. Dresselhaus, Carbon 20 (5) (1982) 427;
See also T. Jawhari, A. Roid, J. Casado, Carbon 33 (11) (1995) 1561.
[20] G. Brunton, D.R. Sears, Acta Crystallogr. B 25 (1969) 2519.